

Tumor-site specific geometric distortions in high field integrated magnetic resonance linear accelerator radiotherapy

Signe Winther Hasler^{a,b,c,*}, Uffe Bernchou^{a,b,c}, Anders Bertelsen^{a,b}, Elisabeth van Veldhuizen^{a,b}, Tine Schytte^{b,c}, Vibeke Nordmark Hansen^{a,b}, Carsten Brink^{a,b,c}, Faisal Mahmood^{a,b,c}

^a Laboratory of Radiation Physics, Odense University Hospital, Klørvænget 19, 5000 Odense C, Denmark

^b Department of Oncology, Odense University Hospital, Klørvænget 19, 5000 Odense C, Denmark

^c Department of Clinical Research, University of Southern Denmark, J. B. Winsløvs Vej 19.3, 5000 Odense C, Denmark

ARTICLE INFO

Keywords:

MRI
MR-linac
Adaptive radiotherapy
MR guided radiotherapy
Geometric distortion
QA

ABSTRACT

Magnetic resonance imaging (MRI) has exquisite soft-tissue contrast and is the foundation for image guided radiotherapy (IGRT) with integrated magnetic resonance linacs. However, MRI suffers from geometrical distortions. In this study the MRI system- and patient-induced geometric distortion at four different tumor-sites was investigated: adrenal gland (7 patients), liver (4 patients), pancreas (6 patients), prostate (20 patients). Maximum level of total distortion within the gross-tumor-volume (GTV) was 0.96 mm with no significant difference between abdominal patients (adrenal gland, liver, pancreas) and pelvic patients (prostate). Total tumor-site specific distortion depended on location in the field-of-view and increased with the distance to MRI iso-center.

1. Introduction

The goal of radiotherapy (RT) is to deliver a high radiation dose to the tumor while sparing surrounding organs at risk (OAR). This is possible with advanced techniques such as intensity modulated RT, volumetric modulated arc therapy, and stereotactic body RT. Image guided RT (IGRT) is used to ensure precise dose delivery [1] and is generally achieved by using cone-beam CT at each treatment fraction, but these images suffer from poor soft-tissue contrast. Magnetic resonance imaging (MRI) has superior soft-tissue contrast and enables visualization of the tumor and OAR, while eliminating ionizing radiation exposure from imaging. MRI based IGRT is made possible with integrated MRI linear accelerators (MR-linac) [2,3].

The MR-linac enables daily in-room adaption of RT treatment plans based on an anatomy-of-the-day strategy acquired with the integrated MRI [4,5]. Fast MRI sequences enable real time imaging during beam-on which allows intra-fractional motion monitoring of the tumor or OAR, and potentially gated treatment delivery [5,6]. Therefore, IGRT not only requires clear visualization of relevant anatomical structures but also a valid geometrical representation of imaged structures to ensure precise dose delivery. Geometric distortion of images is however a well-known problem in MRI [7,8], and is a major concern when MRI is to be used for guidance of RT.

Geometric accuracy can be impaired both by the MRI system and the patient. The important MRI system related sources of distortion are

non-linearity of the spatial encoding gradients (gradient non-linearity, GNL) and inhomogeneity of the main magnetic field (B_0) [8]. Patient-induced geometric distortions arise due to differences in the magnetic susceptibilities of anatomical structures (e.g. air cavities and tissue boundaries) distorting the local B_0 field [9]. Geometric distortion in MR-linacs has been studied by others [9–15], i.e. in the study by Tijssen et al. where a method for cumulative total geometric distortion is presented [10], but larger sample sizes and anatomical tumor-site specific investigation is still warranted. The aim of this study was to investigate the total geometric distortion in a larger sample of patients grouped into anatomical tumor-sites. The total geometric distortion was assessed for clinical scans used in an MRI guided daily adaptive workflow with a 1.5 T MR-linac system. Four different tumor-sites (adrenal gland, liver, pancreas, and prostate) have been evaluated.

2. Materials and methods

2.1. Patients

For this study 37 patients undergoing treatment on the MR-linac were included prospectively. All patients were included in feasibility protocols [16,17] and have given their signed consent to participate. Tumor-sites were: adrenal gland in 7 patients, liver in 4 patients, pancreas in 6 patients, and prostate in 20 patients.

* Corresponding author at: Laboratory of Radiation Physics, Odense University Hospital, Klørvænget 19, 5000 Odense C, Denmark.
E-mail address: signe.winther.hasler@rsyd.dk (S.W. Hasler).

<https://doi.org/10.1016/j.phro.2020.07.007>

Received 28 February 2020; Received in revised form 5 July 2020; Accepted 22 July 2020

Available online 19 August 2020

2405-6316/ © 2020 The Authors. Published by Elsevier B.V. on behalf of European Society of Radiotherapy & Oncology. This is an open access article under the CC BY-NC-ND license (<http://creativecommons.org/licenses/by-nc-nd/4.0/>).

Table 1

Geometric distortions for four tumor-sites. B_0 related distortions and total geometrical distortion (consisting of B_0 and gradient non-linearity (GNL) related distortions) are reported. Median distortion and maximum (defined in section 2.6 *Statistics*) are reported. The sign of the B_0 related distortion reflects the direction of the distortion in the frequency-encoding direction (anterior-posterior direction on images in Fig. 1a–d). The B_0 related distortions are reported for a clinical 3D T2W MRI sequence (specifications can be seen in section 2.3 *B_0 -mapping*). Statistical significant difference between the pooled abdominal tumor-sites (adrenal gland, liver, and prostate) and the pelvic tumor-site (prostate) is denoted by * next to the calculated p-values.

Geometric distortions			B_0				Total			
			GTV		GTV + 30 mm		GTV		GTV + 30 mm	
			Median [mm]	Max [mm]	Median [mm]	Max [mm]	Median [mm]	Max [mm]	Median [mm]	Max [mm]
Abdominal tumor-sites	Adrenal gland	1	0.01	0.08	0.01	-0.06	0.09	0.23	0.09	0.44
		2	-0.01	0.22	0.02	0.10	0.05	0.26	0.09	0.28
		3	0.00	0.24	-0.01	0.21	0.08	0.27	0.10	0.32
		4	0.08	0.13	0.07	0.12	0.09	0.21	0.12	0.28
		5	0.02	0.12	-0.01	0.10	0.13	0.27	0.11	0.33
		6	0.04	0.07	0.03	0.07	0.12	0.31	0.11	0.28
		7	-0.02	0.17	0.01	0.10	0.26	0.48	0.28	0.75
		Mean	0.02	0.15	0.02	0.09	0.12	0.29	0.13	0.38
	Liver	1	0.08	0.13	0.07	0.16	0.21	0.26	0.20	0.52
		2	0.04	0.08	0.05	0.08	0.57	0.67	0.54	1.02
		3	0.02	0.10	0.03	0.10	0.09	0.11	0.08	0.31
		4	0.02	0.15	0.01	0.13	0.44	0.96	0.33	1.27
		Mean	0.04	0.12	0.04	0.12	0.33	0.50	0.29	0.78
	Pancreas	1	-0.01	-0.05	0.01	0.07	0.05	0.12	0.13	0.28
		2	-0.03	-0.08	-0.02	-0.10	0.06	0.14	0.13	0.26
		3	-0.01	-0.05	-0.02	-0.07	0.20	0.28	0.17	0.31
		4	-0.03	0.17	-0.01	0.14	0.20	0.30	0.18	0.37
		5	-0.01	-0.08	0.00	0.07	0.20	0.28	0.16	0.27
		6	-0.03	-0.07	-0.01	0.09	0.13	0.24	0.14	0.28
		Mean	-0.02	-0.03	-0.01	0.03	0.14	0.23	0.15	0.29
Pelvic tumor-site	Prostate	1	-0.05	-0.10	-0.04	-0.14	0.13	0.27	0.12	0.26
		2	-0.06	-0.10	-0.04	-0.09	0.22	0.34	0.11	0.26
		3	-0.03	-0.07	-0.02	-0.08	0.18	0.28	0.10	0.26
		4	-0.01	-0.05	-0.01	-0.06	0.20	0.28	0.10	0.24
		5	-0.01	-0.04	0.01	0.04	0.18	0.26	0.08	0.21
		6	-0.01	-0.07	-0.01	0.07	0.18	0.25	0.10	0.24
		7	-0.03	-0.08	-0.02	-0.07	0.24	0.30	0.10	0.25
		8	-0.04	-0.07	-0.02	-0.08	0.16	0.32	0.10	0.25
		9	-0.03	-0.09	-0.01	-0.06	0.21	0.32	0.09	0.25
		10	-0.05	-0.09	-0.03	-0.07	0.19	0.25	0.09	0.25
		11	-0.02	-0.05	-0.01	-0.06	0.18	0.28	0.10	0.25
		12	-0.03	-0.08	-0.01	-0.07	0.18	0.28	0.09	0.24
		13	-0.04	-0.09	-0.04	-0.08	0.20	0.31	0.10	0.27
		14	0.00	-0.05	0.00	-0.05	0.19	0.29	0.10	0.24
		15	-0.03	-0.07	-0.01	-0.06	0.20	0.30	0.09	0.25
		16	-0.04	-0.08	-0.02	-0.07	0.10	0.21	0.13	0.27
		17	-0.03	-0.08	-0.01	-0.06	0.17	0.32	0.09	0.25
		18	-0.03	-0.07	-0.01	-0.09	0.15	0.27	0.09	0.24
		19	-0.03	-0.08	-0.02	-0.08	0.17	0.26	0.09	0.24
		20	-0.07	-0.12	-0.03	-0.11	0.19	0.30	0.10	0.27
	Mean	-0.03	-0.07	-0.02	-0.06	0.18	0.29	0.10	0.25	
	P-value	< 0.001*	< 0.001*	< 0.001*	< 0.001*	0.20	0.22	0.0013*	< 0.001*	

2.2. MR-linac

All imaging acquisitions were performed on the 1.5 T MR-linac (Unity, Elekta AB, Stockholm, Sweden). A complete user-oriented MR commissioning was performed initially [12] on the MR-linac, including test of overall B_0 -homogeneity, linac gantry rotation dependent distortions, distortions while beam-on and potential eddy currents effects. These effects were found to be negligible.

2.3. B_0 -mapping

B_0 -mapping MRI scans were acquired on the MR-linac. Patients were scanned in treatment position during beam-on at their first treatment fraction. For few cases the B_0 mapping scan was acquired immediately after treatment delivery if motion monitoring images were acquired during the treatment delivery. A 3D gradient echo (GRE) dual-echo MRI sequence was used (TE1/TE2: 4.6/9.2 ms, TR: 11.4 ms, flip angle: 30°)

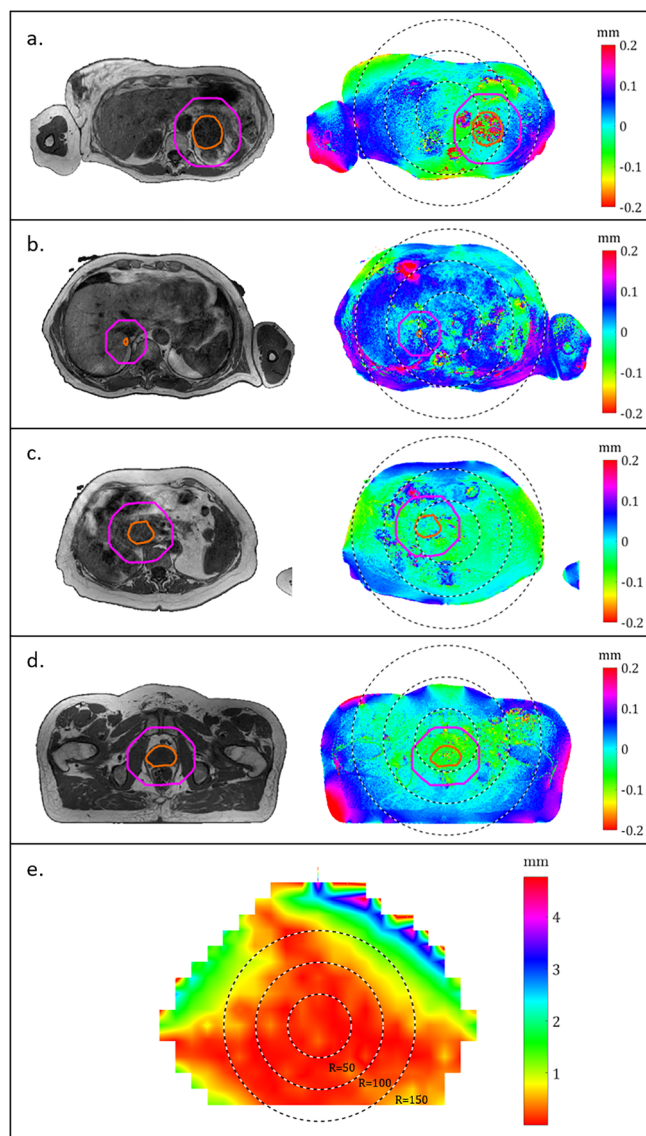


Fig. 1. Representative T2W MRI (left) and corresponding patient-specific B₀ distortion maps (right) (a–d) and system-specific gradient non-linearity (GNL) distortion map for the 1.5 integrated magnetic resonance linac (MR-linac) (e). Red delineations outline gross-tumor-volume (GTV), and magenta delineations outline a 30 mm isotropic margin around GTV. Black dotted lines show concentric circles centered at iso-center and with radii of 50, 100, and 150 mm, respectively. Sign of the B₀ related distortion indicates the direction of the distortion: negative values indicate distortion in the anterior direction and positive distortion indicate distortion in the posterior direction. a: Adrenal gland tumor-site (patient 3), b: liver tumor-site (patient 3), c: pancreatic tumor-site (patient 3), d: prostate tumor-site (patient 2).

with echo times selected to ensure in-phase water-fat-signal to avoid signal cancellation. Magnitude and phase images were acquired with a matrix size of $349 \times 351 \times 229$, readout BW (rBW) of 740 Hz/pixel, and 2 averages resulting in a reconstructed resolution of $0.75 \times 0.75 \times 2 \text{ mm}^3$, and reconstructed matrix of $560 \times 560 \times 229$. Sensitivity encoding (SENSE) was used with reduction factors of 1.5 (frequency encoding (FE)) and 2 (phase encoding (PE)). Percent sampling of the k-space was 78%. Acquisition duration was 406 s. For all acquisitions FE was anterior-posterior (AP) direction, in-plane PE was left–right (LR) direction, and out-of-plane PE was head–feet (HF) direction.

Phase images were unwrapped in 3D using a Laplacian unwrapping algorithm in MATLAB [18,19] and an axial through-tumor slice was used for calculating B₀ maps. B₀ maps were calculated from the

unwrapped phase images with in-house developed software in MATLAB using the dual-echo method [20] where the B₀ variation (ΔB_0) is found from the phase differences ($\Delta\phi$): $\Delta B_0 = \Delta\phi / (2\pi\gamma\Delta TE)$, where γ is the gyromagnetic ratio. The B₀ maps were converted to spatial distortion maps using the rBW (693 Hz/pixel) and the pixel size ($1.2 \times 1.2 \times 2 \text{ mm}^3$) of a clinical 3D T2W spin-echo (SE) sequence for the abdominal/pelvic region.

2.4. GNL mapping

To map the residual GNL related distortion (after 3D system correction) a vendor provided phantom was used (Elekta AB, Stockholm, Sweden). The phantom consisted of 7 slices and each slice contained 274 circular markers located $25 \times 25 \text{ mm}$ apart. GNL was calculated in 2D (central axial plane) using the gradient reversal method [3] (TE: 3.4 ms, TR: 6.7 ms, flip angle: 15°). Magnitude images were acquired with a matrix size of $372 \times 374 \times 200$ and a rBW of 461 Hz/pixel resulting in a reconstructed matrix size of $512 \times 512 \times 400$, and a reconstructed resolution of $1.09 \times 1.09 \times 2 \text{ mm}^3$. The gradient reversal method enabled separation of distortions due to GNL from B₀ induced distortions and a 2D GNL distortion map was created for the central axial slice of the MR-linac which corresponded to the position of the tumor-sites investigated. The GNL distortion map was considered constant and equal in all patients.

2.5. Total distortion

A total distortion map was created for each patient adding the GNL distortion and B₀ distortion contributions. In the FE direction the B₀ related distortion was added to the GNL related distortion. In the PE direction only contribution from GNL existed. Total distortion was found as the magnitude of the added distortion vectors in the FE and PE direction. The median and maximum distortions were reported for the gross tumor volume (GTV) and an expanded region (GTV + 30 mm margin). To remove effects of noise the maximum distortion was reported as the 95-percentile (or 5-percentile if negative) distortion.

2.6. Statistics

Differences in median and maximum distortion between the pooled group of abdominal tumor-sites (adrenal gland, liver, pancreas: 17 patients) and the pelvic tumor-site (prostate: 20 patients) was tested using a Wilcoxon rank-sum test (with $\alpha = 5\%$).

3. Results

The maximum B₀ related distortions inside the GTVs were $< 0.24 \text{ mm}$ for adrenal gland (range 0.07 – 0.24 mm in seven patients), $< 0.15 \text{ mm}$ for liver (range 0.08 – 0.15 mm in four patients), $< 0.17 \text{ mm}$ for pancreas (range $-0.08 - 0.17 \text{ mm}$ in six patients), and $< |-0.12| \text{ mm}$ for prostate (range $-0.04 - -0.12 \text{ mm}$ in 20 patients) (Table 1 and Fig. 1a–d). All results including results for the median values as well as the expanded region can be seen in Table 1. Negative distortions corresponded to a distortion in the anterior direction and positive distortions corresponded to a distortion in the posterior direction. Significant difference (p-values can be seen in Table 1) was seen between the abdominal tumor-sites and the pelvic tumor-site for both median and maximum B₀ related distortion and for both the GTV and expanded region. Difference was due to the direction of the distortion rather than magnitude.

The influence of the systematic GNL distortion depended on the distance of the tumor from the iso-center (Fig. 1e). Maximum total distortion was $< 0.48 \text{ mm}$ for adrenal gland, $< 0.96 \text{ mm}$ for liver, $< 0.30 \text{ mm}$ for pancreas, and $< 0.32 \text{ mm}$ for prostate for the GTVs. For the expanded region the largest distortion was 1.27 mm (liver, patient 4). No significant difference was seen when comparing median and

maximum values for total distortion in GTVs of abdominal tumor-sites and pelvic tumor-sites. When expanding the regions (GTV + 30 mm) significant difference was seen for median and maximum total distortion when comparing abdominal tumor-sites and pelvic tumor-sites.

4. Discussion

The contribution from the B_0 related distortion was generally low, as the highest contribution among the 37 patients was 0.24 mm (adrenal gland, patient 3). Patient-induced distortions in the pelvic region have previously been reported [9,21,22] for different field strengths and receiver bandwidths, which makes direct comparison difficult. Stanescu et al. [9], Glide-Hurst et al. [21] and Tyagi et al. [22] reported values in the same magnitude for tumors/anatomies in the pelvis and prostate. Tijssen et al. reported distortions below 1.5 mm in the abdominal region [10]. As field strength, rBW and pixel size have direct influence on the B_0 related spatial distortion, these parameters need careful consideration in MR guided RT [23].

The median total distortion was not significantly different for the pelvic tumor-site (prostate) compared to the abdominal tumor-sites (adrenal gland, liver, and pancreas). Common for prostate patients the GTV was located within a radius of 50 mm from the MRI iso-center and the contribution from GNL distortion was low (Fig. 1e). The pancreatic tumors were also located near the iso-center, whereas adrenal gland tumors and liver metastasis were located further from the iso-center, which was reflected in a higher GNL related distortion and thereby total distortion. The GNL related distortions were in agreement with results by Kempainen et al. [24]. They reported maximum GNL distortion below 2 mm in most patients, where the tumor-site was close to the iso-center. The largest GNL related distortions in our study was found in two patients with liver metastases (liver, patient 3 and 4, Table 1), at comparable distance to the iso-center. This was in agreement with general deterioration of linearity of the imaging gradient when moving from the iso-center. Liver metastases located farther from iso-center could be affected by GNL related distortions > 2 mm in the MR-linac (Fig. 1e). The GNL contribution was implemented as 2D in-plane in this study. This potentially underestimated the GNL, however, since targets in patients were aligned with the central axial plane the estimation of distortion due to GNL was expected to be sufficiently accurate.

The level of total geometric distortion could be clinically relevant for some of the patients presented, as distortions > 1 mm were seen. Intra-patient variation over time needs to be investigated for the patient-specific B_0 maps to clarify the influence of e.g. patient positioning and air, which could also clarify the usability of patient-specific B_0 maps. The intra-patient variation is a crucial indication for whether B_0 maps should be acquired for each treatment fraction to be relevant, or if a single map at the first treatment is sufficient. To address the consequences of the distortion level for the treatment the dosimetric effect should also be evaluated [25].

In conclusion, the maximum total geometric distortion seen in the GTV was 0.96 mm (liver, patient 4) with no significant difference between abdominal and pelvic patients. The maximum contribution of B_0 related distortion in the GTV was 0.24 mm (adrenal gland, patient 3) and the B_0 related distortion was significantly different in pelvic (prostate) and abdominal tumor-sites (adrenal gland, liver, pancreas). The main source of distortion was due to gradient non-linearity (GNL), and the total distortion level increased as the distance to the MRI iso-center increased. Distortions due to GNL should ideally be taken into consideration if the tumor-site is far off-center in a MR based adaptive RT workflow.

Declaration of Competing Interest

The authors declare that they have no known competing financial interests or personal relationships that could have appeared to influence the work reported in this paper.

Acknowledgement

This work is supported by DCCC Radiotherapy - The Danish National Research Center for Radiotherapy, Danish Cancer Society (grant no. R191-A11526) and Danish Comprehensive Cancer Center, OUH & RH Research Fund (grant no. 58-A2857) and the Danish Cancer Society (grant no. R231-A13852). The funding sources have no other involvement than financial support.

References

- [1] Corradini S, Alongi F, Andratschke N, Belca C, Boldrini L, Cellini J, et al. MR-guidance in clinical reality: Current treatment challenges and future perspectives. *Radiat Oncol* 2019;14:1–12. <https://doi.org/10.1186/s13014-019-1308-y>.
- [2] Mutic S, Dempsey JF. The ViewRay System: Magnetic Resonance-Guided and Controlled Radiotherapy. *Semin Radiat Oncol* 2014;24:196–9. <https://doi.org/10.1016/j.semradonc.2014.02.008>.
- [3] Raaymakers BW, Lagendijk JJW, Overweg J, Kok JGM, Raaijmakers AJE, Kerkhof EM, et al. Integrating a 1.5 T MRI scanner with a 6 MV accelerator: Proof of concept. *54:N229 Phys Med Biol* 2009. <https://doi.org/10.1088/0031-9155/54/12/N01>.
- [4] Raaymakers BW, Jürgenliemk-Schulz IM, Bol GH, Glitzner M, Kotte ANTJ, van Asselen B, et al. First patients treated with a 1.5 T MRI-Linac: Clinical proof of concept of a high-precision, high-field MRI guided radiotherapy treatment. *62:L41 Phys Med Biol* 2017. <https://doi.org/10.1088/1361-6560/aa9517>.
- [5] Bertelsen AS, Schytte T, Møller PK, Mahmood F, Riis HL, Gottlieb KL et al. First clinical experiences with a high field 1.5 T MR linac. *Acta Oncol* 2019;58:1352–7. <https://doi.org/10.1080/0284186X.2019.1627417>.
- [6] Kontaxis C, Bol GH, Stemkens B, Glitzner M, Prins FM, Kerkmeijer LGW, et al. Towards fast online intrafraction replanning for free-breathing stereotactic body radiation therapy with the MR-linac. *Phys Med Biol* 2017;62:7233–48. <https://doi.org/10.1088/1361-6560/aa82ae>.
- [7] Chen Z, Ma CM, Paskalev K, Li J, Yang J, Richardson T, et al. Investigation of MR Image Distortion for Radiotherapy Treatment Planning of Prostate Cancer. *Phys Med Biol* 2005;51:1393–403. <https://doi.org/10.1118/1.1997476>.
- [8] Weygand J, Fuller CD, Ibbott GS, Mohamed ASR, Ding YD, Yang J, et al. Spatial precision in magnetic resonance imaging-guided radiation therapy: The role of geometric distortion. *Int J Radiat Oncol Biol Phys* 2016;95:1304–16. <https://doi.org/10.1016/j.ijrobp.2016.02.059>.
- [9] Stanescu T, Wachowicz K, Jaffray DA. Characterization of tissue magnetic susceptibility-induced distortions for MRIGRT. *Med Phys* 2012;39:7185–93. <https://doi.org/10.1118/1.4764481>.
- [10] Tijssen RHN, Vos R, Philippens MEP, van Lier A, Raaymakers B, van den Berg C et al. Online Geometric Fidelity Inspection for MR-Guided Treatments on 1.5 T MR-Linac: Visualizing the Cumulative Effect of Gradient Errors and Patient Specific Susceptibilities [abstract no. 58]. In: 7th MRinRT Symposium; June 23–25, 2019; Toronto, Canada.
- [11] Goodburn RJ, Tijssen RHN, Philippens MEP. Comparison of Spatial-Distortion Maps for MR-Sim Versus MR-Linac in the Brain and Pelvis at 1.5T [abstract no. EP-2147]. In: ESTRO '37; April 20–24, 2018; Barcelona, Spain.
- [12] Tijssen RHN, Philippens MEP, Paulson ES, Glitzner M, Chugh B, Wetscherek A, et al. MRI commissioning of 1.5T MR-linac systems – a multi-institutional study. *Radiat Oncol* 2019;132:114–20. <https://doi.org/10.1016/j.radonc.2018.12.011>.
- [13] Keesman R, van de Lindt TN, Juan-Cruz C, van den Wollenberg W, van der Bijl E, Nowee ME, et al. Correcting geometric image distortions in slice-based 4D-MRI on the MR-linac. *Med Phys* 2019;46:3044–54. <https://doi.org/10.1002/mp.13602>.
- [14] Nejad-Davarani SP, Kim JP, Du D, Glide-Hurst C. Large field of view distortion assessment in a low-field MR-linac. *Med Phys* 2019;46:2347–55. <https://doi.org/10.1002/mp.13467>.
- [15] Jackson S, Glitzner M, Tijssen RHN, Raaymakers BW. MRI B_0 homogeneity and geometric distortion with continuous linac gantry rotation on an Elekta Unity MR-linac. *Phys Med Biol* 2019;64:12NT01. <https://doi.org/10.1088/1361-6560/ab231a>.
- [16] Schytte T. MR adapted radiotherapy FEASIBILITY study FOR MR LINAC – OUH Institute of Regional Health Research, University of Southern Denmark. <https://open.rsyd.dk/%0AOpenProjects/openProject.jsp?openNo=802&lang=en%0A> [accessed 21 February, 2020].
- [17] Schytte T. The PRISM study-Prostate Radiotherapy with simultaneous MRI, Institute of Regional Health Research, University of Southern Denmark, <https://open.rsyd.dk/%0AOpenProjects/openProject.jsp?openNo=803&lang=uk%0A> [accessed 21 February, 2020].
- [18] Schofield MA, Zhu Y. Fast phase unwrapping algorithm for interferometric applications. *Opt Lett* 2003;28:1194–6. <https://doi.org/10.1364/ol.28.001194>.
- [19] Bouwman JG, Bakker CJG. Alias subtraction more efficient than conventional zero-padding in the Fourier-based calculation of the susceptibility induced perturbation of the magnetic field in MR. *Magn Reson Med* 2012;68:621–30. <https://doi.org/10.1002/mrm.24343>.
- [20] Jezzard P, Balaban RS. Correction for Geometric Distortion in Echo Planar Imaging from B_0 Field Variations. *Magn Reson Med* 1995;34:65–73.
- [21] Glide-Hurst C, Nejad-Davarani S, Weiss S, Zheng W, Chetty IJ, Renisch S. Per-organ assessment of subject-induced susceptibility distortion for MR-only male pelvis treatment planning. *Radiat Oncol* 2018;13:149. <https://doi.org/10.1186/s13014->

- 018-1090-2.
- [22] Tyagi N, Fontenla S, Zhang J, Cloutier M, Kadbi M, Mechalakos J, et al. Dosimetric and workflow evaluation of first commercial synthetic CT software for clinical use in pelvis. *Phys Med Biol* 2018;62:2961–75. <https://doi.org/10.1088/1361-6560/aa5452>.
- [23] Jensen HR, Thomsen JB, Christiansen RL, Bertelsen A, Bernchou U, Brink C, et al. Comparison of Geometrical Distortion in MR Images from of Low-Field and High-Field MR-Linac. *Int J Radiat Oncol Biol Phys* 2019;105:S239. <https://doi.org/10.1016/j.ijrobp.2019.06.348>.
- [24] Kemppainen R, Suilamo S, Tuokkola T, Lindholm P, Deppe MH, Keyriläinen J. Magnetic resonance-only simulation and dose calculation in external beam radiation therapy: a feasibility study for pelvic cancers. *Acta Oncol* 2017;56:792–8. <https://doi.org/10.1080/0284186X.2017.1293290>.
- [25] Gustafsson C, Nordström F, Persson E, Brynolfsson J, Olsson LE. Assessment of dosimetric impact of system specific geometric distortion in an MRI only based radiotherapy workflow for prostate. *Phys Med Biol* 2017;62:2976–89. <https://doi.org/10.1088/1361-6560/aa5fa2>.